Journal of Power Sources 271 (2014) 437–443

Contents lists available at ScienceDirect

Journal of Power Sources

journal homepage: www.elsevier.com/locate/jpowsour

Patterned ion exchange membranes for improved power production in microbial reverse-electrodialysis cells

Jia Liu [a], Geoffrey M. Geise [a, b, c], Xi Luo [d], Huijie Hou [a], Fang Zhang [a], Yujie Feng [e, **], Michael A. Hickner [c], Bruce E. Logan [a, *]

[a] Department of Civil and Environmental Engineering, Penn State University, 212 Sackett Building, University Park, PA 16802, USA
[b] Department of Chemical Engineering, The University of Virginia, 102 Engineers' Way, Charlottesville, VA 22904, USA
[c] Department of Materials Science and Engineering, The Pennsylvania State University, University Park, PA 16802, USA
[d] State Key Joint Laboratory of Environment Simulation and Pollution Control, School of Environment, Tsinghua University, Beijing 100084, PR China
[e] State Key Laboratory of Urban Water Resource and Environment, Harbin Institute of Technology, No. 73 Huanghe Road, Nangang District, Harbin 150090, PR China

HIGHLIGHTS

- Patterned membranes were designed for improved power production in MRCs.
- No spacers were needed due to the hemispherical surface on one membrane side.
- Internal resistance was reduced, increasing power in the MRC.
- Energy recovery and efficiency were also both increased in the MRC.

ARTICLE INFO

Article history:
Received 10 July 2014
Received in revised form
5 August 2014
Accepted 7 August 2014
Available online 14 August 2014

Keywords:
Microbial reverse electrodialysis cell
Patterned membranes
Integrated spacer
Internal resistance

ABSTRACT

Power production in microbial reverse-electrodialysis cells (MRCs) can be limited by the internal resistance of the reverse electrodialysis stack. Typical MRC stacks use non-conductive spacers that block ion transport by the so-called spacer shadow effect. These spacers can be relatively thick compared to the membrane, and thus they increase internal stack resistance due to high solution (ohmic) resistance associated with a thick spacer. New types of patterned anion and cation exchange membranes were developed by casting membranes to create hemispherical protrusions on the membranes, enabling fluid flow between the membranes without the need for a non-conductive spacer. The use of the patterned membrane decreased the MRC stack resistance by ~22 Ω, resulting in a 38% increase in power density from 2.50 ± 0.04 W m^{-2} (non-patterned membrane with a non-conductive spacer) to 3.44 ± 0.02 W m^{-2} (patterned membrane). The COD removal rate, coulombic efficiency, and energy efficiency of the MRC also increased using the patterned membranes compared to the non-patterned membranes. These results demonstrate that these patterned ion exchange membranes can be used to improve performance of an MRC.

1. Introduction

Salinity gradient energy is recognized as a large and sustainable source of energy. The amount of power that could be captured globally from naturally occurring salinity gradients, such as river water and seawater, has been estimated to be 1.9–2.6 TW [1,2]. Reverse electrodialysis (RED) is one of several technologies being investigated to capture and convert salinity gradient energy into useful power. The RED process is based on a stack of alternating anion membranes (AEMs) and cation exchange membranes (CEMs) that separate high (HC) and low salt concentration (LC) solutions. When HC and LC solutions are fed into the RED stack, a potential difference is created across the membranes (e.g., ~0.1–0.2 V per cell

* Corresponding author. Tel./fax: +1 814 863 7908.
** Corresponding author. Tel./fax: +86 451 86287017.
E-mail addresses: yujief@hit.edu.cn (Y. Feng), blogan@psu.edu (B.E. Logan).

http://dx.doi.org/10.1016/j.jpowsour.2014.08.026
0378-7753/

pair [3,4]), which can drive redox reactions at the electrodes and generate electricity. However, a large number of cell pairs are normally needed to overcome high electrode overpotentials and produce net power [5,6]. The use of many cell pairs not only increases the capital cost of the RED stack, but also increases energy consumption for pumping solutions through a large number of membrane channels due to high solution resistance [7].

A microbial reverse electrodialysis cell (MRC), which combines a microbial fuel cell (MFC) and a RED stack [8], recently emerged as a sustainable water treatment technology that can harvest chemical energy from organic matter and at the same time extract electrical energy from salinity gradients [9]. MFC electrodes can be used to spontaneously generate electrical current when exoelectrogenic bacteria metabolize organics in wastewater and release electrons, and oxygen in air is reduced at the cathode [10,11]. When MFC electrodes are used with a RED stack, providing favorable reactions at the electrodes, energy can be efficiently extracted by MRC stack using only a small number of membrane pairs. The inclusion of the MRC stack also improves the performance of the MFC electrodes, resulting in synergistically-enhanced power production compared to each individual process [8]. Further MRC performance improvement requires reducing the internal resistance of the MRC stack. For example, two membrane pairs of a small MRC stack accounted for nearly two-thirds (63%) of the total internal resistance of the MRC stack [12]. Reducing MRC stack resistance could substantially improve MRC performance and the efficiency of energy extraction from salinity gradients.

The internal resistance of the RED part of MRC reactor can be reduced by minimizing the space between the membranes [6,13]. In an MRC stack the inter-membrane distance is determined by the spacer thickness. Spacers are used to distribute the flow evenly across the membrane surface, and maintain separation between the membranes. The spacer thickness directly determines the ohmic resistances of HC and LC solutions [1], and therefore, decreasing the inter-membrane distance (by decreasing the spacer thickness) increases performance [14]. Commonly used spacers, made from nylon [5,14], polyethylene (PE) [8], and polyamide [15] polymers, are not ion-conductive materials. Non-conductive spacers mask a part of the ion exchange membrane area and block ion transport. This “shadow effect” of the spacer can increase internal stack resistance and lower power output [6,16]. The use of ion-conductive spacers in MRC can avoid this impact of surface coverage with a non-conductive material and improve MRC stack performance, but the spacers must be thin to avoid high solution resistances.

The use of patterned membranes has recently been proposed as a promising method to avoid the use of separate spacers in a RED stack and to minimize electrode spacing [17,18]. Patterned membranes examined so far had straight-ridge, wave or pillar structures that were integrated into the membrane design, allowing solution flow through these structures without the need for non-ionically conductive spacers [17,19]. Since the patterned structures are ion conductive, there is no shadow effect. The use of patterned membranes can therefore increase the area available for ion transport, and when properly designed, reduce the laminar boundary layer resistance to ion transport and increase the higher power density compared to that of flat membranes with spacers [17,19,20]. Although a variety of different structures of the patterned membranes have been used in RED [20,21] or electrodialysis (ED) [17], patterned structures membranes have so far not been examined for use in MRCs. Here we prepared patterned ion exchange membranes based on making hemispherical protrotrusions on one side of the membrane, and demonstrated that their use in MRCs increased the energy recovery and efficiency of the process by reducing inter-membrane distances and the membrane stack internal resistance.

2. Materials and methods

2.1. Patterned and smooth membrane fabrication

Poly(phenylsulfone) (Radel R-5500, M_w = 63 kg mol^{-1}, dry density = 1.29 g cm^{-3}) was kindly provided by Solvay Advanced Polymers, LLC. Poly(vinyl alcohol-*co*-ethylene) (PVA-co-PE), poly(-vinylbenzyl chloride) (PVBC), *N*,*N*-dimethylacetamide (DMAc, anhydrous, 99.8%), and *N*,*N*,*N*′,*N*′-tetramethyl-1,6-hexanediamine (99%) were purchased from Sigma–Aldrich, Inc. (USA) and were used without further purification. Polydimethylsiloxane (PDMS) (Sylgard 184) was obtained from Dow Corning, Inc. (MI, USA). A polytetrafluoroethylene (PTFE) plate was purchased from McMaster-Carr, (OH, USA).

Poly(phenylsulfone) was sulfonated [22] to prepare the cation exchange membrane polymer. The solution used to cast the cation exchange membrane (CEM) was prepared by first drying sulfonated poly(phenylsulfone) under vacuum for 24 h. Then, 1.50 g of this polymer was dissolved in DMAc (35 mL, anhydrous) at room temperature. The polymer solution used to make the anion exchange membrane (AEM) was prepared in four steps. First, 10.0 g PVA-co-PE was mixed with 90 mL DMAc. The solution was stirred at 80 °C for 2 h to allow the PVA-co-PE to completely dissolve. The solution was allowed to cool to room temperature and was filtered using a 5.0 μm PTFE filter. Next, 10.0 g PVBC was dissolved in 90 mL DMAc at room temperature for 20 min. Then, 3.75 mL *N*,*N*,*N*′,*N*′-tetramethyl-1,6-hexanediamine was added to 31.25 mL DMAc. Finally, aliquots the three solutions, PVA-co-PE (6.81 mL), *N*,*N*,*N*′,*N*′-tetramethyl-1,6-hexanediamine (2 mL), and PVBC (1.7 mL) were mixed with DMAc (7.5 mL) and were stirred for 10 min.

The patterned membranes were made by casting the CEM and AEM polymer solutions using a micromachined PTFE mold (Fig. 1). The base of the mold was constructed from a block of PTFE (7 cm × 7 cm × 3 cm width) that was micro-machined to contain 200 hemispherical holes (diameter: 300 μm, spacing: 2 mm). PDMS precursor solution (7 g, Sylgard 184) (10:1 ratio (v/v) with the curing agent of Sylgard 184 silicone elastomer curing agent) was dispensed on the base of the mold and then degassed using a vacuum oven to remove bubbles from the holes, and cured at 60 °C for 2 h. The polymerized PDMS was removed from the PTFE mold and reversed, creating an inversed replica of the PTFE mold with extruded hemisphere microstructures. The PDMS slab was then used as mold for membrane casting. The CEM or AEM polymer solution (10 mL) was poured into the PDMS mold and cured for 2 d at 35 °C (AEM) or at 50 °C (CEM) in an oven, producing the final patterned ion exchange membrane. The same process was used to prepare the smooth membrane (Fig. S1), except a smooth PTFE tray was used.

2.2. MRC construction and operation

The MRC reactor consisted of separate anode and cathode chambers separated by an MRC stack (Fig. 2). The anode chamber was made of a 4 cm long polycarbonate cubic block drilled to contain a cylindrical chamber (3 cm diameter). The cathode chamber was made the same way but it was only 2 cm long [8]. The anodes were heat-treated graphite fiber brushes (2.5 cm diameter × 2.5 cm length; PANEX 33 160 K, ZOLTEK), that were placed vertically in the middle of the anode chamber [23]. The air cathodes were made of carbon cloth (projected cross sectional area of 7 cm^2) as previously described, with four diffusion layers made of PTFE on the air side, and a Pt/C catalyst layer (10% Pt on Vulcan XC-72, Fuel cell store) on the solution side [24]. Both anode and cathode chambers contained Ag/AgCl reference electrodes (Bioanalytical Systems, Inc., RE-5B; +0.209 V versus a standard

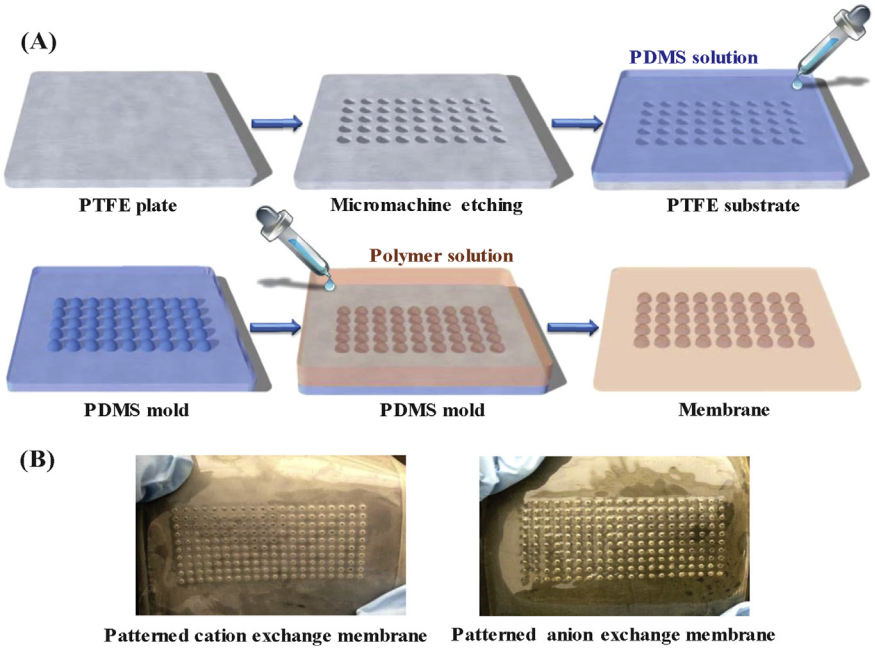

Fig. 1. (A) Schematic of the fabrication process of the membrane with integrated spacer; (B) photographs of patterned CEM and AEM.

hydrogen electrode, SHE) to measure electrode potentials and stack voltages.

The MRC stack with the patterned membranes was compared to a stack made with smooth membranes and a non-conductive spacer. The stacks contained 2 AEMs and 1 CEM (Fig. 2). The patterned membranes were 0.2 mm apart due to the height of the hemispherical protrusions (Fig. 2B). The spacer used in the stack containing smooth membranes (Fig. 2A) was a 1.3 mm thick polyethylene mesh, resulting in a separation distance between the membranes that was more than 6 times greater than that used in the profiled membrane stack [8]. The HC solution was 35 g L^{-1} NaCl (54 mS cm^{-1}), while the LC solution was 0.35 g L^{-1} (0.72 mS cm^{-1}), resulting in a salinity ratio of 100. The HC and LC solutions were pumped (peristaltic pump, MPII, Harvard Apparatus, MA) into the smooth membrane stack containing the spacers at a flow rate of 0.8 mL min^{-1} (0.05 cm s^{-1}) [7]. In order to maintain the same flow velocity (0.05 cm s^{-1}) along the membrane surface as that used for the spacer membrane tests [15,16], the HC and LC solutions were pumped into the patterned membrane stack at a flow rate of 0.13 mL min^{-1}.

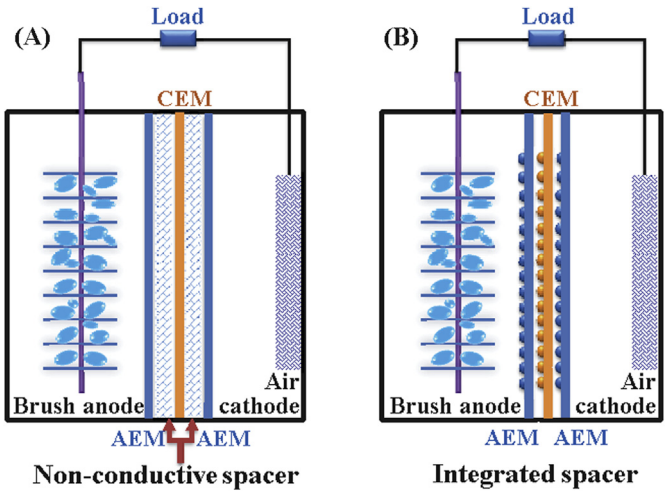

Fig. 2. Schematic of the MRCs with: (A) conventional, non-conductive spacers (smooth membrane with spacer, MRC-S); and (B) integrated spacer (patterned membrane without spacer, MRC-P). (CEM, cation exchange membrane; AEM, anion exchange membrane).

The MRC anodes were first acclimated in single chamber, air-cathode MFCs at a fixed external resistance of 1000 Ω. These MFCs were inoculated with the effluent of an MFC operated for over one year. After reproducible stable voltage production was obtained for at least five successive fed-batch cycles, anodes were transferred into the MRC reactors [25]. The anolyte consisted of 1 g L^{-1} sodium acetate as the fuel in a 100 mM bicarbonate buffer solution (BBS) containing $NaHCO_3$, 8.4 g L^{-1}; NH_4Cl, 0.31 g L^{-1}; KCl, 0.13 g L^{-1}; Na_2HPO_4, 0.05 g L^{-1}; $NaH_2PO_4 \cdot H_2O$, 0.03 g L^{-1}; trace minerals, 12.5 mL L^{-1} and vitamins, 5 mL L^{-1} [26]. The catholyte was a 0.6 M sodium bicarbonate solution. All MRCs were operated with a 100 Ω external resistance unless otherwise noted, in a constant temperature room (30 °C).

2.3. Calculations and measurements

The cell voltage (U) across the external resistor (Load, Fig. 2) was recorded at 20 min intervals using a data acquisition system (Model 2700, Keithley Instrument, Cleveland, OH). Polarization curves were obtained using the single-cycle method by varying the external circuit resistance in a decreasing order with 20 min intervals at each resistance (from open circuit potential to 25 Ω) [24]. Ag/AgCl reference electrodes were separately placed into the anode and cathode chambers to measure electrode potentials. The anode (R_{an}), cathode (R_{cat}) and stack resistances (R_{stack}) were calculated from the slopes of the polarization data by linear regression of the curves. The stack resistance was separated into different components using galvanostatic electrochemical impedance spectroscopy (GEIS): solution and membrane ohmic resistance within the stack (R_{s+m}), electric double layer resistance (R_{DL}) and diffusion boundary layer resistance (R_{DBL}). Current was set at 1.5 mA, over a frequency

range of 50 mHz–1 MHz with a sinusoidal perturbation of 0.1 mA amplitude [27].

The power densities were calculated as $P = U^2/R_{ex}A_{cat}$, and current densities were calculated as $I = U/R_{ex}A_{cat}$, where A_{cat} was normalized to the projected surface area of the cathode (7 cm^2). Coulombic efficiency (CE) was calculated based on COD removal as previously described [28]. Energy recovery (r_E) was calculated from total energy applied versus energy recovered, while energy efficiency (η_E) was based on energy calculated for the anode and saline solutions entering and leaving the reactors as previously described [8,14]. The membrane thickness was the average thickness obtained using an electronic micrometer (3732XFL-1 Starrett®, USA). Membrane area resistance was measured using a DC current method (membrane is exposed on either side to the 0.5 mol L^{-1} NaCl solution) [29]. The ion exchange capacities (IECs) and membrane ionic resistance were measured as previously described [30].

3. Results and discussion

3.1. Membrane characteristics

The patterned membranes were 370 ± 10 μm thick, with raised hemispherical protrusions on the patterned membranes 150 ± 10 μm high, while the smooth membranes were 220 ± 10 μm thick (Table 1). The patterned AEM resistance was 3.0 ± 0.1 Ω cm^{-2}, compared to 2.7 ± 0.1 Ω cm^{-2} for the smooth membranes. The patterned CEM resistance was 8.3 Ω cm^{-2}, which was 13% higher than that of the smooth membrane. The IEC of the membranes provides information about the degree of ionic functionalization of the polymer. The IEC of the CEM was 1.7 meq g^{-1} and 2.0 meq g^{-1} for the AEM membrane. These IECs are larger than typical commercial ion exchange membranes, such as those made by Fumasep (CEM, 0.6–1.0 meq g^{-1}, AEM, 1.0–1.5 meq g^{-1}). Additionally, the membranes used in this study were thicker than state of the art commercial ion exchange membranes, which are typically around 100 μm thick, so thinner profiled membranes would be expected to have even lower membrane resistances compared to those reported here.

3.2. MRC operation

The MRCs were operated for several cycles, with highly reproducible current profiles produced over several successive fed-batch cycles (Fig. 3A). The MRC with patterned membranes (MRC-P) produced a maximum peak current of 7.39 ± 0.04 mA (100 Ω external resistance), which was 34% higher than that obtained using the smooth membranes with non-conductive spacers (MRC-S) (5.53 ± 0.03 mA). The electrode potentials were nearly identical (Fig. 3B), and therefore differences in current production were due to the differences in the RED stacks. The whole cell voltage of the RED stack with the patterned membranes initially increased more rapidly than the smooth membranes due to higher current production, and therefore more rapid depletion of the fuel.

Table 1
Properties of patterned (P) and smooth (S) membranes. (CEM, cation exchange membrane; AEM, anion exchange membrane; R_m, area resistance; IEC, ion exchange capacity. Error bars ± SD were based on averages measured in triplicate.)

Membrane	Thickness (μm)	R_m (Ω cm^2)	IEC (mequiv g^{-1})
CEM-S	218 ± 10	7.4 ± 0.1	1.7
CEM-P	377 ± 5	8.3 ± 0.1	1.7
AEM-S	223 ± 8	2.7 ± 0.1	2.0
AEM-P	369 ± 10	3.0 ± 0.1	2.0

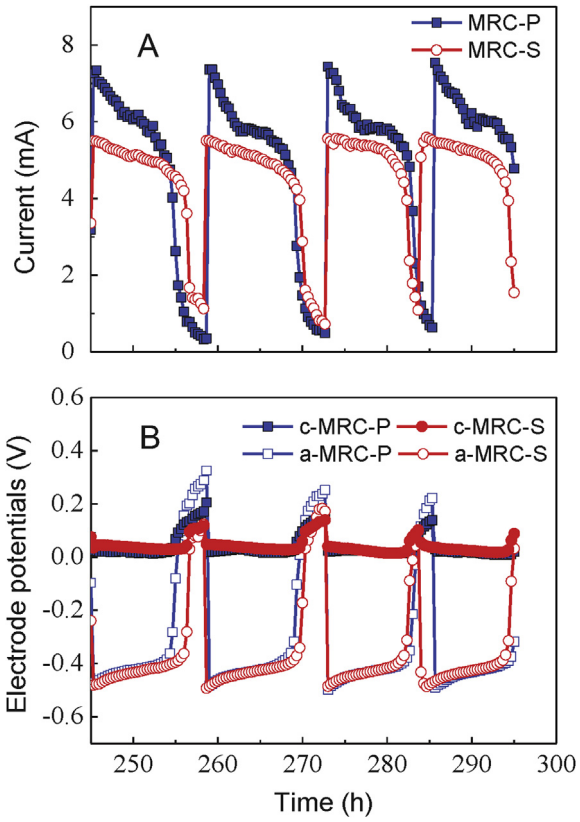

Fig. 3. (A) Current generation, and (B) electrode potentials versus Ag/AgCl reference electrode for the MRC using different membranes with a non-conductive spacer (MRC-S) or integrated patterned spacer (MRC-P). (a, anode potential; c, cathode potential).

Polarization and power density results also showed that the MRC with the patterned membranes performed better than the MRC with the smooth membranes. The maximum power density for the MRC-P was 3.44 ± 0.02 W m^{-2}, compared to 2.50 ± 0.04 W m^{-2} for the MRC-S (Fig. 4A). This power density of MRC-P is a substantial improvement compared to previous MRC results, as less power was obtained (3.0 W m^{-2}) despite the use of a stack with 11 membranes (same reactor configuration with same salinity ratio of 100, brush anode and Pt/C cathode) [8] compared to only 3 membranes here.

The voltage of the cell was produced by spontaneous half cell reactions at both electrodes, and the membrane Donnan potentials of the stack ($E = E_{cat} - E_{an} + E_{stack}$). The anode and cathode potentials of both MRC-P and MRC-S were nearly identical (Fig. 4C), indicating that improved performance with the patterned membrane was due to the membrane stack and not the electrodes. The stack open circuit voltages were similar at 0.2 V with either type of membrane, but with current generation the stack with patterned membrane had higher stack voltage than the one with the smooth membrane (Fig. 4B). The stack voltage decreased with increasing current density due to the stack internal resistance. The stack therefore contributed to the total power production only until the stack reached its limiting current, where the stack voltage was now 0 V. As current production was driven by the spontaneous reactions at the anode and the cathode, current densities exceeded the stack limiting current density, resulting in the stack being a net consumer of power. The limiting current of the stack with the patterned membranes was 5.2 A m^{-2}, compared to 3.6 A m^{-2} with the smooth membranes, and thus the stack with the patterned membranes produced more power than the smooth membranes.

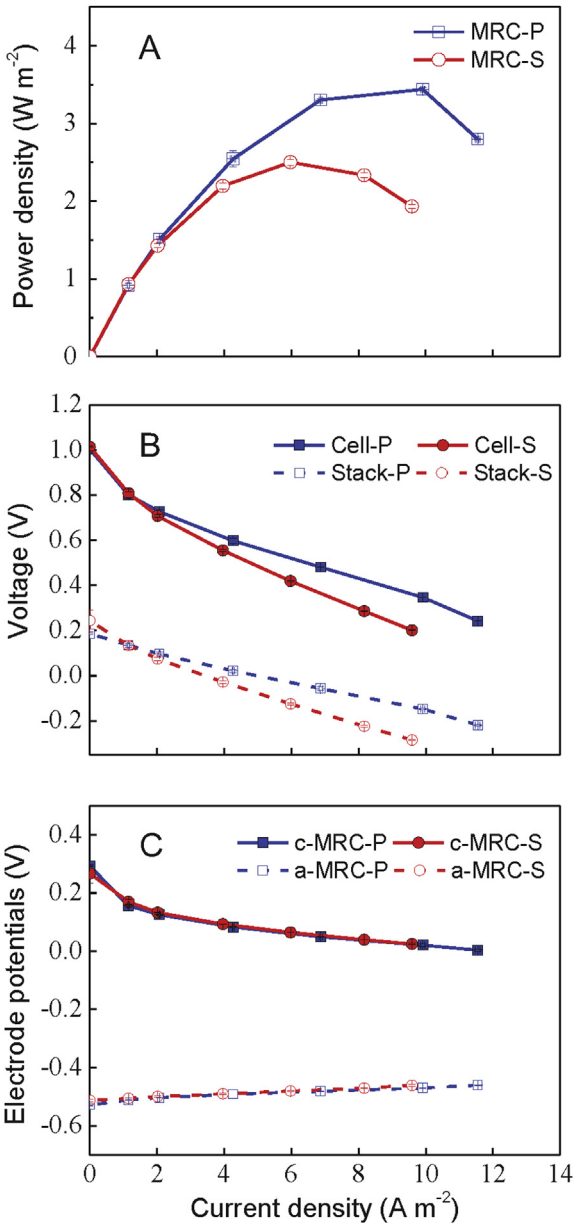

Fig. 4. (A) Power density curves, (B) polarization and MRC stack potentials, and (C) electrode potentials versus current density for the MRC using different membranes with a non-conductive spacer (MRC-S) or integrated patterned spacer (MRC-P). (a, anode potential; c, cathode potential).

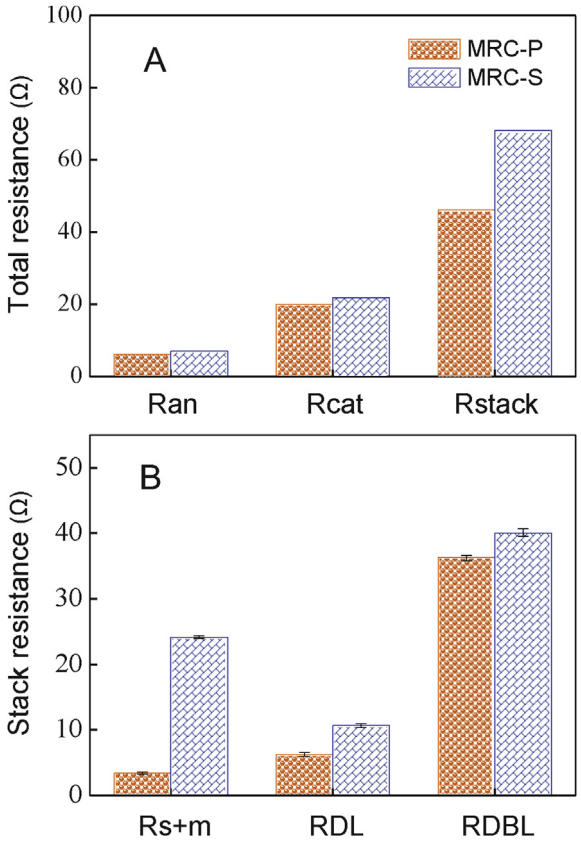

Fig. 5. (A) The total internal resistance of the MRC, which is the sum of the anode (R_{an}), cathode (R_{cat}), and stack resistances (R_{stack}) (calculated using the slope of the polarization curve for the MRC); (B) Individual components of the stack resistance determined using galvanostatic electrochemical impedance spectroscopy (GEIS): solution and membrane (R_{s+m}), double layer (R_{DL}), and diffusion boundary layer (R_{DBL}). MRC-P, MRC with the patterned membranes; MRC-S, MRC with a non-conductive spacer.

3.3. Internal resistance analysis

The differences in performance were reflected in the changes in the internal resistance of the MRC stacks. The MRC-P had an internal resistance 46.1 ± 0.6 Ω, while the MRC-S had a resistance that was 48% higher, or 68.1 ± 2.0 Ω (Fig. 5A). The electrode resistances of the stack with the patterned membranes (R_{an} = 6.3 ± 0.2 Ω, and R_{cat} = 20.1 ± 0.2 Ω) were essentially the same as those of the MRC with the smooth membranes and spacers, as expected from lack of differences in electrode potentials.

The predominant resistance for both patterned membrane MRC-P and the smooth membrane MRC-S was the diffusion boundary layer resistance (R_{DBL}) (Fig. 5B). The double layer resistance (R_{DL}) only marginally contributed to the resistance. The R_{DBL} of the patterned membrane MRC-P (36.3 ± 0.4 Ω) was slightly lower than that of the smooth membrane MRC-S (40.1 ± 0.6 Ω), indicating that the hemispherical protrusion structure of the patterned membranes resulted in an effective disruption of the boundary layers [18,20]. The membrane and solution ohmic resistance (R_{s+m}) with the patterned membrane MRC-P was greatly reduced compared to that the smooth membrane MRC-S. For the smooth membrane MRC-S, the R_{s+m} was 24.2 ± 0.2 Ω, which was ~6.1 times higher than that using the patterned membrane MRC-P (3.4 ± 0.1 Ω). It was expected that the patterned membranes provided a conductive path for ion transport [17,18], which eliminated the spacer shadow effect and hence reduced the R_{s+m} for the MRC-P. Additionally, the LC chamber (e.g., river water) has a large contribution to the internal resistance of the stack due to the low salt concentration [14]. The LC chamber of the MRC-P was much thinner than that of the MRC-S due to the use of patterned membranes, which could significantly reduce the LC solution resistance, thus resulting in a much lower solution ohmic resistance within the stack.

3.4. COD removal and coulombic efficiency

The average COD removals (86 ± 2%) and coulombic efficiencies (88 ± 1%) of the MRC with the patterned stacks were slightly higher than those obtained using the smooth membranes (COD removals of 82 ± 2% and CE of 83 ± 2%) (Fig. 6A). The higher coulombic efficiency was likely a result of the higher current density of the MRC-P than the MRC-S, although the cycle time was not a factor as they were stopped at the same time. With a higher current, more of the

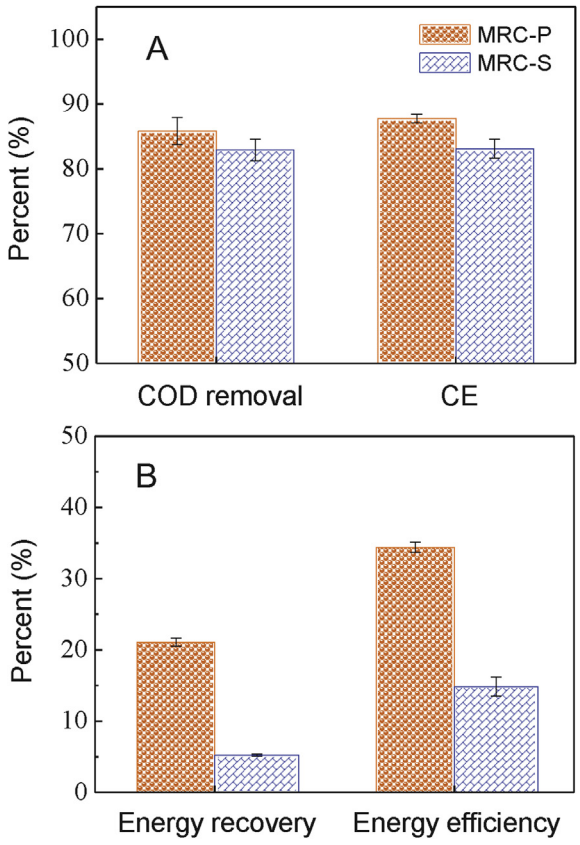

Fig. 6. (A) COD removal, coulombic efficiency; (B) energy efficiency and energy recovery for the MRC using different membranes with a non-conductive spacer (MRC-S) or integrated patterned spacer (MRC-P).

fuel is diverted into current generation rather than being lost to other processes, such as microbial aerobic respiration using oxygen leaking through the cathode or methanogenesis [31]. The reason for the slightly higher COD removal is less clear, but it could be due to the result of the stack driving the anode to process more substrate over the cycle length.

3.5. Energy efficiencies and energy recoveries

The energy efficiencies and recoveries of the MRC-P were significantly higher than those of the MRC-S (Fig. 6B). The energy efficiency based on the energy entering minus leaving of $\eta_E = 35 \pm 1\%$ was observed for the MRC-P, which was 1.3 times larger than that using the MRC-S with non-conductive spacer (15 ± 1%). The energy efficiency of the MRC-P is comparable to that obtained for the RED systems (10%–35% when neglecting the energy loss due to electrode reactions) [5]. Comparing the MRC-P and MRC-S, the much smaller inter-membrane distance of the MRC-P enabled the use of a lower flow rate, which resulted in a smaller salinity gradient energy input (based on entering minus leaving) for the MRC-P (0.00079 W) than that for the MRC-S (0.0055 W). Thus, the relatively higher power production and lower energy input of the MRC-P resulted in a larger energy efficiency compared to the MRC-S.

Energy recovery based on the total energy applied to the system was $r_E = 21 \pm 1\%$ for the MRC-P, which was about ~3 times larger than that using the MRC-S with a non-conductive spacer (5.2 ± 0.1%). The energy recovery of 21% of MRC-P was also significantly higher than that previously reported for an MRC with 5 cell pairs ($r_E = 10\%$) [8]. This high energy recovery for the MRC-P was mainly due to the low flow rate used here, which resulted in a much smaller total salinity gradient energy input (based on total supplied) for the MRC-P (0.004 W) than that for the MRC-S (0.025 W) or the MRC with 5 cell pairs (0.024 W) [8].

The pressure drop, and thus the energy needed for pumping, was dependent on the inter-membrane distance. The energy consumption for water pumping through the membranes of the MRC-P was estimated to be 9.5×10^{-3} W m^{-2}-membrane, which was about ~4.6 times larger than the using MRC-S (1.7×10^{-3} W m^{-2}-membrane). This energy loss of MRC-P is <1% of the maximum power generation per membrane (0.97 W m^{-2}-membrane). Thus, the energy loss for pumping was relatively negligible for the MRC operation.

4. Conclusions

Patterned ion-exchange membranes with integrated spacers were prepared and applied for the first time in an MRC system, and power density increased while internal resistance decreased compared to smooth membranes with non-conductive spacers. This patterned membrane system had a higher energy efficiency (34 ± 1%) and energy recovery (21 ± 1%) relative to that using the smooth membranes ($\eta_E = 15 \pm 1\%$, $r_E = 5.2 \pm 0.1\%$). Although the use of patterned membranes reduced the inter-membrane distance and increased pumping energy consumption, the net energy consumption for water pumping was relatively negligible (<1%). Thus, this patterned membrane could enable the design of more effective MRCs for wastewater treatment and capture of salinity gradient energy.

Acknowledgments

We thank Weihua He for help with the analytical measurements. This work was supported by Award KUS-I1-003-13 from the King Abdullah University of Science and Technology (KAUST), the State Key Laboratory of Urban Water Resource and Environment, Harbin Institute of Technology (Grant No. 2013DX08), the National Natural Science Foundation of China for Distinguished Young Scholars (51125033), National Funds for Creative Research Group of China (Grant No. 51121062) and Science and Technology Cooperation Project Between the Government of Canada and China (2011DFG96630).

Appendix A. Supplementary data

Supplementary data related to this article can be found at http://dx.doi.org/10.1016/j.jpowsour.2014.08.026.

References

[1] J.W. Post, H.V.M. Hamelers, C.J.N. Buisman, Environ. Sci. Technol. 42 (2008) 5785–5790.
[2] G.Z. Ramon, B.J. Feinberg, E.M.V. Hoek, Energy Environ. Sci. 4 (2011) 4423–4434.
[3] J. Veerman, M. Saakes, S.J. Metz, G.J. Harmsen, Environ. Sci. Technol. 44 (2010) 9207–9212.
[4] J.N. Weinstein, F.B. Leitz, Science 191 (1976) 557–559.
[5] J. Veerman, R.M. de Jong, M. Saakes, S.J. Metz, G.J. Harmsen, J. Membr. Sci. 343 (2009) 7–15.
[6] P. Dlugolecki, A. Gambier, K. Nijmeijer, M. Wessling, Environ. Sci. Technol. 43 (2009) 6888–6894.
[7] Y. Kim, B.E. Logan, Proc. Natl. Acad. Sci. U. S. A. 108 (2011) 16176–16181.
[8] Y. Kim, B.E. Logan, Environ. Sci. Technol. 45 (2011) 5834–5839.
[9] R.D. Cusick, Y. Kim, B.E. Logan, Science 335 (2012) 1474–1477.
[10] B.E. Logan, Nat. Rev. Microbiol. 7 (2009) 375–381.
[11] D.R. Lovley, Curr. Opin. Biotechnol. 17 (2006) 327–332.
[12] R.D. Cusick, M. Hatzell, F. Zhang, B.E. Logan, Environ. Sci. Technol. 47 (2013) 14518–14524.
[13] J.W. Post, J. Veerman, H.V.M. Hamelers, G.J.W. Euverink, S.J. Metz, K. Nymeijer, C.J.N. Buisman, J. Membr. Sci. 288 (2007) 218–230.

[14] D.A. Vermaas, M. Saakes, K. Nijmeijer, Environ. Sci. Technol. 45 (2011) 7089–7095.
[15] J. Veerman, M. Saakes, S.J. Metz, G.J. Harmsen, J. Membr. Sci. 327 (2009) 136–144.
[16] P. Dlugolecki, J. Dabrowska, K. Nijmeijer, M. Wessling, J. Membr. Sci. 347 (2010) 101–107.
[17] J. Balster, D.F. Stamatialis, M. Wessling, J. Membr. Sci. 360 (2010) 185–189.
[18] D.A. Vermaas, M. Saakes, K. Nijmeijer, J. Membr. Sci. 453 (2014) 312–319.
[19] E. Guler, R. Elizen, M. Saakes, K. Nijmeijer, J. Membr. Sci. 458 (2014) 136–148.
[20] D.A. Vermaas, M. Saakes, K. Nijmeijer, J. Membr. Sci. 385 (2011) 234–242.
[21] D.A. Vermaas, M. Saakes, K. Nijmeijer, Electrochim. Acta 117 (2014) 9–17.
[22] T. Saito, M.D. Merrill, V.J. Watson, B.E. Logan, M.A. Hickner, Electrochim. Acta 55 (2010) 3398–3403.
[23] Y.J. Feng, Q. Yang, X. Wang, B.E. Logan, J. Power Sources 195 (2010) 1841–1844.
[24] J. Liu, Y.J. Feng, X. Wang, Q. Yang, X.X. Shi, Y.P. Qu, N.Q. Ren, J. Power Sources 198 (2012) 100–104.
[25] X. Luo, J.Y. Nam, F. Zhang, X.Y. Zhang, P. Liang, X. Huang, B.E. Logan, Bioresour. Technol. 140 (2013) 399–405.
[26] J. Liu, Y.J. Feng, X. Wang, X.X. Shi, Q. Yang, H. Lee, Z.H. Zhang, N.Q. Ren, J. Power Sources 196 (2011) 8409–8412.
[27] M.C. Hatzell, B.E. Logan, J. Membr. Sci. 446 (2013) 449–455.
[28] J. Liu, Y.J. Feng, W.H. He, Y.Y. Gong, Y.P. Qu, N.Q. Ren, J. Power Sources 248 (2014) 317–322.
[29] G.M. Geise, A.J. Curtis, M.C. Hatzell, M.A. Hickner, B.E. Logan, Environ. Sci. Technol. Lett. 1 (2014).
[30] G.M. Geise, M.A. Hickner, B.E. Logan, ACS Appl. Mater. Interfaces 5 (2013) 10294–10301.
[31] L. Ren, X. Zhang, W. He, B.E. Logan, Biotechnol. Bioeng. (2014), http://dx.doi.org/10.1002/bit.25290.